

Characterization of reversibly switchable fluorescent proteins (rsFPs) in optoacoustic imaging

Paul Vetschera^{a,b,+}, Kanuj Mishra^{a,+}, Juan Pablo Fuenzalida-Werner^a, Andriy Chmyrov^{a,c}, Vasilis Ntziachristos^{a,b,c} and Andre C. Stiel^{a,*}

^a) Institute of Biological and Medical Imaging (IBMI), Helmholtz Zentrum München, Neuherberg, Germany

^b) Chair of Biological Imaging, Technische Universität München, Munich, Germany

^c) Center for Translational Cancer Research (TranslaTUM), München, Germany

⁺) These authors contributed equally

^{*}) Correspondence should be addressed to A.C.S. (andre.stiel@helmholtz-muenchen.de)

ABSTRACT

Reversibly switchable fluorescent proteins (rsFPs) have had a revolutionizing effect on life science imaging due to their contribution to subdiffraction-resolution optical microscopy (nanoscopy). Initial studies showed that their use as labels could also be highly beneficial for emerging Photo- or Optoacoustic imaging. It could be shown that their use in Optoacoustics i) strongly improves the imaging CNR due to modulation and locked-in detection, ii) facilitates fluence calibration affording precise measurements of physiological parameters and finally iii) could boost spatial resolution following similar concepts as used for nanoscopy. However, rsFPs show different photophysical behavior in optoacoustics than in optical microscopy because optoacoustics requires pulsed illumination and depends on signal generation via non-radiative energy decay channels. This implies that rsFPs optimized for fluorescence imaging may not be ideal for optoacoustics. Here, we analyze the photophysical behavior of a broad range of rsFPs with optoacoustics and analyze how the experimental factors central to optoacoustic imaging influence the different types of rsFPs. Finally, we discuss how knowledge of the switching behavior can be exploited for various OA imaging approaches using sophisticated temporal unmixing schemes.

INTRODUCTION

Reversibly switchable fluorescent proteins (rsFPs) are a class of mostly green fluorescent protein (GFP)-like transgene imaging labels that can be selectively and reversibly switched between metastable states with distinct photo-physical characteristics by light of appropriate different wavelengths (for review see ¹). The on/off-switching of fluorescence, possible with rsFPs, revolutionized optical imaging due to its importance for subdiffraction-resolution microscopy concepts (nanoscopy) ^{2,3}. Structural studies as well as photophysical analysis allowed for tailored improvements of rsFPs for nanoscopy (for overviews see: ⁴⁻⁶).

Photo- or Optoacoustic (OA) imaging is an innovative imaging approach that overcomes the penetration depth limit of optical imaging methods by acoustically detecting light absorption ⁷⁻⁹. In contrast to light, ultrasound waves are only weakly scattered in tissue, thus the resolution of optoacoustic images is limited only by ultrasound diffraction, not photon diffusion. The contrast in optoacoustic imaging is based on the different absorption coefficients of tissue components like blood, melanin and lipids or suitable transgene labels in the sample. Those absorbers can be separated by multiwavelength illumination and subsequent unmixing algorithms ¹⁰. The method allows high-resolution imaging of tissue to depths of several centimeters ^{11,12} and has already proved effective at imaging brain activity ^{13,14}, precise cancer localization ^{15,16} and cell-fate and migration of macrophages ¹⁷ or stem-cells ¹⁸. However, longitudinal, non-invasive studies of live animals, one of the unique capabilities of optoacoustic imaging, are limited by the low number of transgene labels

for optoacoustic and their poor signal generation efficiency, which complicates imaging of specific processes at the cellular and sub-cellular level¹⁹. The relatively weak optoacoustic signals generated by illuminating transgene labels at single wavelengths results in weak contrast compared to other strong absorbers like hemoglobin or melanin.

Recently, a method was described for harnessing the unique properties of rsFPs as transgene labels in optoacoustic imaging: Light-driven modulation of the rsFPs, together with lock-in detection of the optoacoustic signals, could strongly improve the contrast-to-noise ratio (CNR) especially over the background of abundant endogenous absorbers like hemoglobin²⁰⁻²². Moreover, this approach also allows temporal unmixing of different labels and therefore multiplexing with only two wavelengths²¹. Additionally, recent studies could show that the characteristic light-intensity dependent switching kinetics of rsFPs can be used to calibrate light fluence which can improve the accuracy of e.g. blood-oxygenation measurements with optoacoustics²³; or metastable rsFPs can be used to selectively mark cell populations as demonstrated for photoconvertible proteins²⁴. Finally, imaging schemes similar to nanoscopy can improve the spatial resolution²⁰. However, these studies already suggested that the different illumination (pulsed) and detection (ultrasound) leads to a different behavior of rsFPs in optoacoustic compared to fluorescence imaging. This implies that rsFPs optimized for fluorescence imaging may not be ideal for optoacoustics, and it highlights the need for systematic analysis of rsFPs in the optoacoustic modality in order to provide a baseline for further protein engineering efforts to enhance their performance.

Switching in rsFPs relies on the light-driven transition between distinct states that differ in chromophore planarity, stability and protonation. These factors determine the absorption and fluorescence spectra of each switched state (exemplified for Dronpa: ^{25,26}). Two major types can be distinguished (Figure 1): photochromic rsFPs that show a change in absorption spectra upon switching (photochromes) and rsFPs that exhibit a quantum yield (QY) change but largely preserve the absorption spectra (QY-changer). Presently, the majority of rsFPs stem from the class of GFP-like FPs, showing absorption in the green, yellow and red regions of the spectrum⁴. Recently, the class of bacteriophytochromes harboring a porphyrin chromophore have found attention as labels in the near-infrared (NIR)²⁷. Members of this class are reversibly switchable similar to classic photochromic rsFPs, but they have not been largely exploited for imaging^{20,22}. Like any other chromophore rsFPs show a number of possible deexcitation pathways of their excited state. Predominant are the fast processes internal-conversion (ps) and fluorescence (ns) as well as processes associated with the eponymous switching like *cis/trans* isomerization and/or photoinduced protonation/deprotonation²⁸ (ms for Dronpa-like²⁹). Intersystem-crossing and subsequent triplet deexcitation by quenching, phosphorescence or radiationless decay ($\mu\text{s} - \text{s}$, for Dronpa-like²⁶) have often only a smaller contribution for GFP-like proteins³⁰ although a connection with switching especially photo-conversion is discussed^{28,31}.

This is especially true for the pulsed illumination used in our study with ns pulse length and < 100 Hz repetition rates. The major contributor to the observable optoacoustic signal is the relaxation from the S1 by internal-conversion occurring on the ps timescale. Other events that can dissipate heat happen on a longer timescale ($\gg 1 \mu\text{s}$) and would produce signals that have only neglectable contributions in the bandwidth of our transducer. All these processes are competitive to internal conversion, thus despite we cannot directly measure them, the various alternative deexcitation pathways impact the observable PGE. Moreover, this value is not only influenced by the direct photophysics but also by the immediate proteins surrounding, especially the shielding beta-barrel of FPs enclosing the chromophore, can create a microenvironment with different

thermoelastic parameters than the bulk solvent³². However, all these parameters are convoluted in the observable PGE and thus allow for a comparative study.

Presently a broad range of rsFP have been used for fluorescence imaging, but only a few rsFPs have been used for optoacoustic applications. In this work we systematically analyze the characteristics of rsFPs in terms of optoacoustic signal generation, switching kinetics and applicability for optoacoustic imaging. Additionally, we elucidate the differences that optoacoustic imaging imposes on the switching behavior of those proteins and provide a conceptual framework to predict rsFP characteristics in optoacoustic imaging. Although far-red rsFPs may be most promising for deep-tissue optoacoustic imaging, we analyzed a broad range of rsFPs differing substantially in absorbance spectra, switching directionality and switching timescales in order to provide a more comprehensive understanding of how experimental conditions affect the photophysics of these promising labels in optoacoustic. Our goal is to provide a rational basis for developing rsFPs specifically for optoacoustic imaging, rather than co-opting labels previously optimized for fluorescence imaging.

EXPERIMENTAL SECTION

Cloning. rsFPs were a kind gift from Prof. Stefan Jakobs (Max Planck Institute for biophysical chemistry and University of Göttingen, Germany) or synthesized as gene strings (GeneArt, LifeTechnologies, Regensburg, Germany). The coding sequence of rsFPs Dronpa, DronpaM159T, rsFastlime, Padron, rsCherry, rsCherryRev, rsCherryRev1.4 and rsTagRFP was subcloned using XhoI/HindIII into a Arabinose inducible pBad-HisA vector while BphP1 was subcloned in the second multiple cloning site of pET-Duet1 using restriction sites NdeI/XhoI. Additionally, for Biliverdin synthesis for BphP1, the heme oxygenase of *Nostoc sp.* was cloned using NcoI/HindIII in the first multiple cloning site of pET-Duet1.

Protein Expression and purification. Proteins have been expressed in *E. Coli* strains Top10 and BL21 using standard protocols, respectively. After cell lysis, all proteins were purified by metal affinity chromatography (IMAC), followed by desalting using a Sephadex G-25 resin HiPrep 26/10 column (GE Life Sciences, Freiburg, Germany).

Optoacoustic measurements. Before measurement proteins were diluted to similar Q-band optical densities in the equilibrium state. Purified RSFP were characterized with a custom-made experimental set-up shown in Supporting Information (Figure S1). Nanosecond excitation pulses were generated by an optical parametric oscillator (OPO) laser (Spitlight-DPSS 250 ZHG-OPO, Innolas, Germany) running at a repetition rate of 50Hz (raw laser intensities vs. wavelength can be found in Supporting Information (Figure S2). Constant pulse energy was ensured using a half wave plate in a motorized rotation stage (PRM1Z8, Thorlabs, Germany) and a polarizing beam splitter; using a lookup table and adapting the polarization with the halfwave-plate, we kept the power constant at ~ 1.3 mJ over the whole illumination spectrum. A motorized filter wheel with a low pass and a high pass filter at 700nm was used to remove the near-infrared (NIR) and visible (VIS) fraction in the laser pulses generated by the OPO. Samples were injected into an acoustically coupled flow chip (μ -Slide I 0.2 Luer, hydrophobic, uncoated, IBIDI, Germany) and illuminated from one side using a fiber bundle (CeramOptec, Germany) at a constant pulse energy of ~ 1.3 mJ at the fiber output. Optoacoustic signals were detected using a cylindrically focused single-element transducer (V382-SU, 3.5 MHz, Olympus, Germany) and averaged over 10 laser pulses to improve the SNR. A second flow chip in the light path with low concentrated indian ink was used for the generation of reference signals to correct for any deviation in the measurement approach. Briefly: Before plotting the OA spectrum and calculation of the average OA value of each wavelength, the 10 OA peak-to-peak signals of the sample

at each wavelength are divided by the 10 normalized ink reference peak-to-peak signals of their respective time transients. We confirmed the linearity and stability of the optoacoustic signal generated by indian ink in the range of fluences used in our experiments and compared it to other well established optoacoustic reference compounds³³ (Supporting Information, Figure S3). The optoacoustic signals were amplified by 60dB using a wideband voltage amplifier (Femto, Germany) and digitized at 100MS/s with a data acquisition card (RZE-002-400, GaGe, USA). Exemplary wave functions of our optoacoustic signal can be found in Supporting Information (Figure S4). The waveform is virtually identical, so no other heat realizing process take place on the time scale of our transducer detection^{34,35}. We further show this data in frequency space (Figure S5) showing the same result with major contributions from frequencies around 0.3 MHz. Moreover, when considering the loss of energy via fluorescence decay, none of our proteins shows an acoustic signal generation significantly higher than our standard (which shows maximal thermal conversion)^{36,37}, so most likely no photochemical reaction producing a volume contribution is taking place^{34,35}.

Absorption spectra were recorded after each excitation wavelength by fast interruption of the laser pulse illumination with an electronic shutter (SHB1, Thorlabs, Germany) and opening the shutter of a fiber-coupled broadband white light illumination lamp (DH-2000, Ocean Optics). Triggering for both shutters was provided by micro-controller (Arduino uno, USA). Detection of the transmission spectra was provided by a commercial UV-VIS spectrometer (USB 4000, Ocean Optics). The setup has a time delay for the absorption measurement of at least 110 ms after the laser pulses due to shutter responses. Both, the illumination and the detection fiber were attached to a collimator rotated by 45° to the optoacoustic illumination-detection axis. Each absorption transmission spectrum was averaged over 20 acquisitions. For the optoacoustic spectra measurements, ten optoacoustic time transients at each wavelength at 5nm steps were recorded. To correct for laser pulse energy deviations, the peak-to-peak values at each wavelength were divided by the normalized peak-to-peak signals generated by the reference microfluidic chip which were clearly separated in time from the sample signals. The noise level was corrected by shifting minimum of the uncorrected optoacoustic spectrum to zero. Shift between visible and infrared spectral measurements for BphP1 have been corrected using copper sulfate³⁸. For the absorption measurements, the measured transmission spectra were divided by the spectrum of a reference microfluidic chip filled with phosphate buffered saline (PBS) and then subtracted from a ones vector to obtain the relative absorption. Consequently, the absorption spectra were averaged over 5nm to visualize the same spectral resolution as for the optoacoustic spectra. Baseline shifts due to light fluence deviations introduced by the white light lamp were corrected by shifting the baseline to zero. ON-state spectra were consequently normalized and the respective peaks visually matched to the corresponding optoacoustic spectrum. OFF-state spectra were equally normalized and subsequently matched to ON/OFF peak ratio of the averaged non-normalized absorption raw data.

For Figure 1 and Supporting Information, Figure S8 show two different features of the recorded absorbance spectra. In Fig. 1, the whole wavelength range of the spectrum after multiple averaging at the onset of the switching cycle is presented. In Supporting Information, Figure S8, fractions of the absorbance spectrum after laser illumination of the corresponding wavelength are averaged over 5nm (e.g. 497.5-502.5nm after 500nm illumination) and subsequently concatenated to the full spectrum.

Switching cycles were recorded by the optoacoustic peak-to-peak values as a function of laser pulses. Cycle plots in figure 2 are averaged over 20 consecutive pulses. The excitation wavelengths chosen for switching were selected as close as possible to the absorption peak maxima. For BphP1, 630nm and 780nm were chosen to avoid the overlapping wavelength range of the two states.

Overall temperature stability in the sample chamber was ensured by monitoring the peak-to-peak distances of the optoacoustic measurement which are indicative of the speed-of-sound and hence the temperature of the sample (Supporting Information, Figure S6B). Moreover, we used a thermo-camera with 0.05°C sensitivity (FLIR E60, FLIR Systems GmbH, Germany) to monitor the overall temperature in the water-bath used for coupling (Supporting Information, Figure S6C).

Pulsed vs. Continuous bleaching experiments. Bleaching experiments were performed using a laser diode at 450nm with a custom-built laser diode driver described in ³⁹. The diode was triggered using a commercial waveform generator (Rigol, Germany) with rectangular pulses with a pulse duration/repetition rate of 10ns/50MHz, 100ns/5MHz and 1000ns/500kHz respectively. Continuous-wave (CW) illumination was generated with a duty cycle of 99.9%. The output of the laser diode was directly attached to a multimode fiber. Before the experiment, the power for all the pulse durations was measured with a powermeter (Thorlabs, Germany) and the amplitude of the triggering pulses was adjusted to ensure 500μW power for all pulse durations at the output of the fiber. Purified sfGFP protein was inserted in a coverslip and illuminated for 300s. Fluorescence signals were bandpass-filtered from 500 to 570 nm and detected with an avalanche photodiode (SPCM-AQRH-13, Excelitas, Canada) and digitized at a sampling rate of 100 samples/s with a data acquisition card (PCIe-6353, National Instruments, USA). The mean noise level was subtracted from the data and subsequently the fluorescence signal amplitude was normalized and its minimum set to zero.

RESULTS AND DISCUSSION

In choosing the rsFPs for this work we tried to cover a representative range of this protein class (Figure 1 and Table 1, ^{4,20,47,25,40–46}). However, we focused on the derivatives of the green rsFP Dronpa ⁴⁸ since this group combines proteins with different switching kinetics and directionality at similar wavelengths whose photophysics have been extensively studied. We analyzed all proteins using a unique custom-built spectrometer setup (Supporting Information, Figure S1) equipped with a tunable (420 – 2100 nm) pulsed laser with a repetition rate of 50 Hz, pulse duration of 7 ns and energies of ~ 1.3 mJ which allowed us to record high-quality optoacoustic spectra (Supporting Information, Figure S6) in conjunction with the absorption spectra (see experimental section for details).

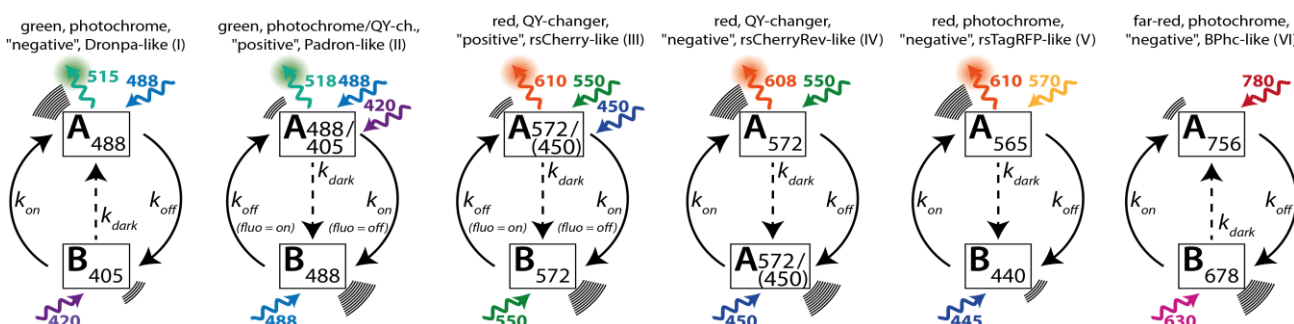


Figure 1. Switching schemes of the studied rsFPs. Light excitation and emission is denoted with a curled arrow labeled with the corresponding wavelength. For fluorescence emission the average wavelength of all proteins in this group is given. Emission of ultrasound is indicated by curved lines, with the number of lines indicating relative strength of emission. Switching states, A and B are given with the respective wavelength of their excitation maximum; for rsFP classes with several members, the most common laser wavelength in this spectral range was selected. State transitions are denoted with full arrows for light driven transitions and dashed arrows for dark state relaxation. Note that in the case of b and c, the classic switching directions in fluorescence imaging are reversed in optoacoustics.

Table 1. Overview of photophysical parameters of rsFPs covered in this study.

rsFP	Absorption maxima (nm)	Emission maxima (nm)	quantum yield (QY)	Molar absorption coefficient ($M^{-1} \cdot cm^{-1}$)	switching mode	equilibrium state fluorescence	Continuous illumination (i.e. for fluorescence excitation) illumination (<u>only values from one source are intercomparable!</u>)		dark relaxation half-time $t_{1/2}^{dark}$ (s)	Pulsed illumination (1.3 mJ/pulse, 7 ns pulse length, 50 Hz repetition rate)	OA switching dynamic range	Bleaching $t_{1/2}$ (min)	photo acoustic signal generation (PGE) in equilibrium state rel. to $CuSO_4^*$	photo acoustic signal generation (PGE) in switched state rel. to $CuSO_4^*$
							switch-on half-time $t_{1/2}^{on}$ (s) *	switch-off half-time $t_{1/2}^{off}$ (s) *						
Dronpa^a	503 / 390 ^a	518 ^a	0.85 ^a , 0.67 ^k	95,000 ^a	negative	100 % ^d	0.1 ^b , 0.12 ^d (405)	263 ^b , 115 ^d (488)	50,400 ^b	19.78	0.57	n.d.	0.03 (485)	n.d.
rsFastLime^b	496 ^b / ~390	518 ^b	0.77 ^b , 0.60 ^d	39,094 ^b , 46,000 ^d	negative	93 % ^d	0.11 ^b , 0.03 ^d (405)	5 ^b , 2.6 ^d (488)	480 ^b	5.81	0.68	29	0.06 (485)	n.d.
Dronpa-M159T^b, Dronpa-2^c	489 ^b / ~390	515 ^b	0.23 ^b , 0.33 ^c , 0.28 ^k	61,732 ^b , 56,000 ^k	negative	~100 %	0.05 ^b (405)	0.23 ^b (488)	30 ^b	0.64	0.89	55	0.68 (485)	n.d.
Padron^d	503 / 396 ^d	522 ^d	0.64 ^d	43,000 ^d	positive	5 % ^d	5.6 ^d (488)	0.06 ^d (405)	9000 ^d	4.99	0.61	36	0.62 (500)	0.49 (510)
rsEGFP2^e	478 / 408 ^e	503 ^e	0.3 ^e	61,300 ^e	negative	~100 %	-	0.0005 ^e (488)	-	1.78	0.88	17	0.46 (485)	n.d.
rsCherry^f	572 ^f / ~405	610 ^f	0.02 ^j	80,000 ^f	positive	32 % ^f	3 ^f (550)	0.05 ^f (450)	40 ^f	16.49	0.28	64	0.74 (570)	0.69 (570)
rsCherryRev^f	572 ^f / ~405	608 ^f	0.0051 ^l	42,300 ^f , 84,000 ^k	negative	8 % ^f	0.05 ^f (450)	0.7 ^f (550)	13 ^f	n.d.	n.d.	n.d.	0.47 (570)	n.d.
rsCherryRev1.4^g	572 / 450 ^g	609 ^g	-	-	negative	~8 %	-	-	-	n.d.	n.d.	n.d.	0.46 (570)	n.d.
rsTagRFP^h	565 / 440 ^h	585 ^h	0.11 ^h	36,800 ^h	negative	33 % ^h	0.0028 ^h (440)	0.18 ^h (570)	~3300 ^h	14.16	0.91	25	0.45 (570)	n.d.
BphP1ⁱ	756 / 678 ⁱ	n.a. ⁱ	n.a. ⁱ	78,300 ⁱ	negative	n.a. ⁱ	-	-	-	0.65	0.9	> 200	0.31 (755)	0.53 (685)

"~" = approximations made by the authors

"." = no data available in literature

"n.d." = data not defined in this study

*) wavelength for switching or PGE determination is given in brackets in nm

a) Ando R., *Science*, 2004

b) Stiel A.C., *Biochem. J.*, 2007

c) Ando R., *Biophys. J.*, 2007

d) Andresen M., *Nat. Biotechnol.*, 2008

e) Grotjohann T., *eLIFE*, 2012

f) Stiel A.C., *Biophys. J.*, 2008

g) Lavoie-Cardinal F., *ChemPhysik*

h) Subach F.V., *Chemistry & Biology*

i) Yao J., *Nat. Methods.*, 2015

j) Shcherbakova D.M., *Annu. Rev. Biophys.*, 2014

*) Zhou, X.X., *Curr. Opin. in Chem. Biol.*, 2013

Optoacoustic and absorption spectra characteristics. In contrast to fluorescence detection, a low QY and thus a high level of non-radiative de-excitation favors the generation of optoacoustic signals (photoacoustic generation efficiency, PGE). To determine the PGE and analyze spectral characteristics of rsFPs we recorded optoacoustic as well as absorbance spectra of the equilibrium state and, where possible, the switched state (Figure 2). In general, the spectral shape of optoacoustic and absorbance spectra coincides very well (R^2 higher than 0.94) with only minimal differences observed in the case of proteins showing very low optoacoustic signal (e.g. Dronpa, $R^2=0.80$; Figure 2d). The absorbance spectra depicted in Figure 2 is an averaging of several absorbance spectra at the onset of each switching cycle. A comparison with the absorbance at each wavelength measured simultaneously with the respective wavelength in the optoacoustic spectra can be found in supporting information (Figure S8). Differences directly relate to the influence of QY and to a lesser extend other decay channels on the PGE and allow us to quantify its contribution for the different proteins. rsEGFP2, Dronpa-M159T (Dronpa 2), rsFastlime, Dronpa, rsTagRFP and *Rhodospseudomonas palustris* Bacteriophytochrome (BphP1) are proteins with switching predominantly governed by photochromism (Figure 2e, a, b, c, i and j). For these proteins, upon switching, the optoacoustic spectra closely follow the absorbance spectra resulting in optoacoustic signal differences between the on and off states of $\sim 100\%$ for Dronpa-M159T, rsEGFP2, rsTagRFP and BphP1 as well as $\sim 90\%$ for rsFastLime, resulting in a high dynamic range of switching (Table 1). rsFastlime shows an absorbance in the 488-state after switching, which however cannot be seen in the optoacoustic spectra possibly hinting to a residual 488-population with very low fluorescence and PGE. This could be a state with high positional freedom prior to isomerization. Despite Dronpa being equally switchable like e.g. Dronpa-M159T the slow switching of the wildtype protein could not be resolved in our optoacoustic spectra (see below, section switching), moreover the high QY leads to very low PGE complicating the measurement.

In contrast to the photochromes, the switching of rsCherryRev and its sibling rsCherryRev1.4 (Figure 2g and 2h) is dominated by changes in QY. Accordingly, we see no change in absorbance spectra upon switching, however, also the change in QY of the already poorly fluorescent proteins results in too small a change in the optoacoustic spectra to be resolved by our optoacoustic spectrometer (see below, section switching).

Padron and rsCherry (Figure 2d and f) show a combination of QY change and photochromism with the switched spectra exhibiting a lower absorbance at 488 nm and 550 nm, respectively, but a higher QY. This is clearly reflected in higher optoacoustic signal for those switched states with dynamic ranges of $\sim 50\%$ and $\sim 20\%$, respectively. As a result, the two proteins that are positive switchers for fluorescence (i.e. irradiation with excitation wavelength switches on) are negative switchers for optoacoustics, since both the lowered absorbance and increased QY have detrimental effects on the optoacoustic signal. We used absorption data and the optoacoustic signal of the same sample at similar wavelengths to calculate the PGE (Table 1). In general, fluorescent proteins present an absorption spectrum with the main band exhibiting a blue-shifted shoulder. As can be observe in Supporting Information (Figure S9), the PGE of this shoulder when calculate by its own absorbance is significantly lower than that of the main peak. This phenomenon is stronger in red proteins.

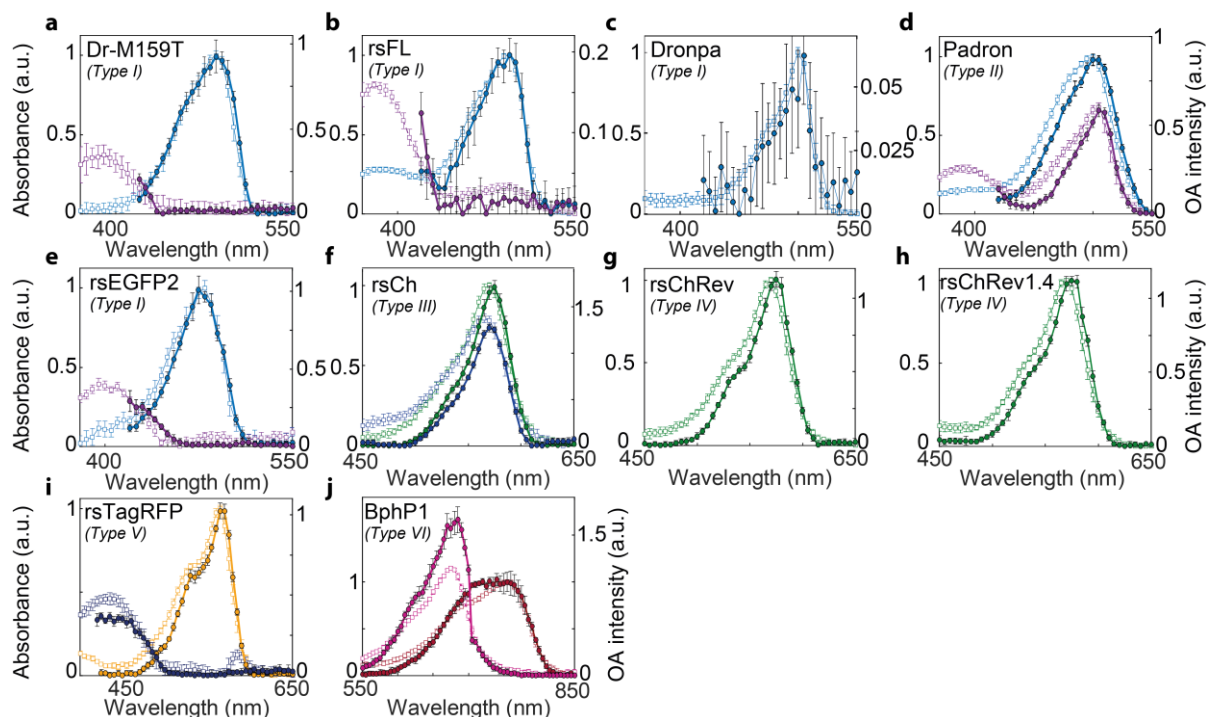


Figure 2. Optoacoustic (solid) and absorbance (thin / hollow) spectra of rsFPs in both switched states. Optoacoustic and absorbance spectra are chosen to ease comparison of the spectral features. The coloring of the curves refers to the switched states, respectively. All spectra are normalized to the absorbance state of the equilibrium spectra, defined as 1. The switching mode as described in Figure 1 is denoted in the upper left corner of each plot. For Dronpa (d), rsCherryRev (g) and rsCherryRev1.4 (h), no spectral change was observable upon switching. Optoacoustic and absorbance spectra that have been recorded completely simultaneous and are shown in Supporting Information (Figure S8). Abbreviations: Dr = Drona, rsFL = rsFastlime, Ch = Cherry.

As described previously⁴⁹ the optoacoustic signal generation is inversely linked to the QY. Dronpa, with a very high QY of 0.85, shows the weakest optoacoustic signal with a PGE < 0.1 while the poor QY of 0.3 and 0.23 of rsEGFP2 and Dronpa-M159T result in PGEs of ~ 0.5 and ~ 0.7 , respectively. Moreover, rsCherryRev, exhibiting a very low QY of 0.005,⁴ shows also only a PGE of ~ 0.5 , hinting that small changes in QY are negligible for optoacoustics. Interestingly, the two “positive” rsFPs Padron and rsCherry show higher PGEs than their respective relatives Dronpa-M159T and rsCherryRev, despite exhibiting comparable or even higher QY. It is interesting to note that positive rsFPs are described as having a more space-conserving isomerization route for their chromophores involving fewer rearrangements in the vicinity of the chromophore^{25,50}. Whether this is connected to the different PGE remains to be elucidated. Overall the data show that photochromic rsFPs can provide a high dynamic range in optoacoustics, whereas QY-change rsFPs, especially those with initially low QY, support only infinitesimal optoacoustic signal modulation.

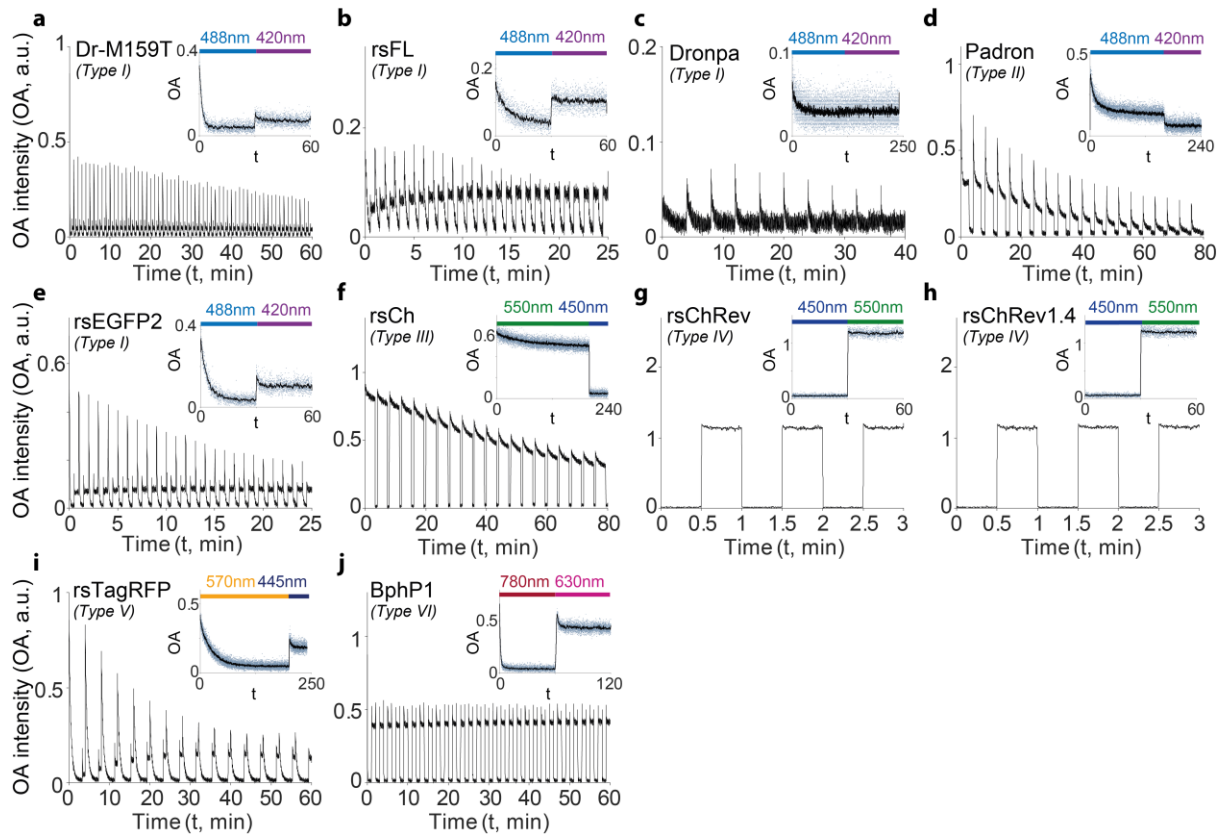


Figure 3: Change of optoacoustic signal of rsFPs upon switching with light of different wavelengths. Shown are several switching cycles per protein. Insets show a single cycle with the used excitation and switching light denoted as a bar above the trace. Abbreviations as in Figure 2.

Switching rsFPs in optoacoustics. Switching behavior under optoacoustic (i.e. pulsed) illumination is the crucial factor determining the usability of an rsFPs in optoacoustics. We recorded switching kinetics of all rsFPs by multiple cycles of alternating switching wavelengths (Figure 3, see Figure 1 for details on the switching schedule and mode). The studied green rsFPs provide a set that allows direct comparison of switching kinetics under comparable illumination. The trend known from fluorescence switching with kinetics ranging from slow-switching Dronpa to fast-switching Dronpa-M159T and rsEGFP2 is also observable in optoacoustics. However, the overall switching at the given repetition rate of 50 Hz is much slower than in fluorescence imaging (Figure 4). This can be attributed to the pulsed illumination used in optoacoustics. Depending on the repetition rate of the laser, only a small part of the pulse provides illumination while the remaining time the sample is dark. Since the switched states in rsFPs are metastable and naturally relax in the absence of illumination to their equilibrium state, the dark time between pulses allows partial recovery of the equilibrium state, effectively counteracting the switching. We demonstrated this dependency by switching with three different laser repetition rates (10, 25, 50 Hz, Figure 4A). The switching half-time increased from ~ 5 s at 50 Hz to ~ 25 s at 10 Hz. For high-repetition laser systems, the effect of the natural relaxation between pulses is negligible. A measurement of rsEGFP2 with a 20 MHz repetition rate shows switching half-times of 0.4 ms \pm 0.1 ms (Supporting Information, Figure S10). Both results match well with a theoretical approximation of the switching and recovery under pulsed illumination using two-exponential functions (Figure 4A).

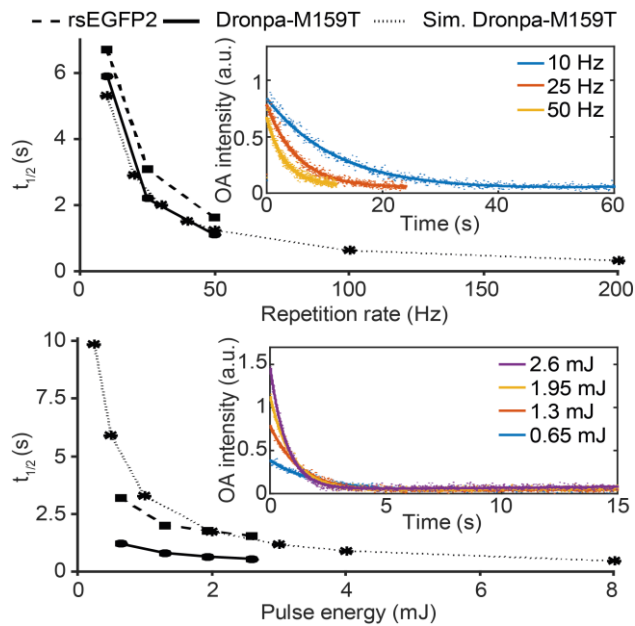


Figure 4. Dependency of switching times on laser repetition rate (a) and laser energy (b) for rsEGFP2 and Dronpa-M159T as well as predicted development for Dronpa-M159T (dotted line). The insets show exemplary switching behavior for Dronpa-M159T at different repetition rates or pulse energies, respectively.

Photo-fatigue of rsFPs under optoacoustic illumination. Photo-fatigue (permanent bleaching or long-lived dark states) is an essential parameter in every imaging experiment since it limits the maximal dwell time. We determined the number of possible switching cycles for our set of rsFPs under our illumination conditions (Figure S11). For the GFP-like rsFPs, Dronpa-M159T shows the least bleaching. However, it is clearly surpassed by the far-red bacteriophytochrome BphP1. Towards elucidating the general difference between continuous and the pulsed energy deposition used in optoacoustics we compared the photo-fatigue of superfolder GFP (sfGFP)⁵¹ under four illumination conditions of at the same power: 10 ns/50 MHz (pulse width / repetition rate), 100 ns/5 MHz, 1 μ s/500 kHz and continuous, all deposited the same power of 500 μ W, allowing comparison (Figure 5). We selected a non-switchable protein for this experiment in order not to confound switching with photo-fatigue. The results show an accelerated bleaching for pulsed illumination, which scales inversely with the pulse length. This effect could be attributed to multiple photons absorbed by each chromophore, resulting in transitions to long-lived or photolytic higher-order singlet and triplet states S_n and T_n ⁵².

As for fluorescence, switching kinetics in optoacoustics show an exponential dependence on illumination intensities (Figure 4B). For the rsFP derivatives of mCherry the change of QY upon illumination is the major source of fluorescence modulation. For fluorescence this results in sufficient signal modulation, but for optoacoustics, the small change from low to even lower QY translates to infinitesimal signal changes. Most rsCherry and rsCherryRev molecules are off in the equilibrium state, which translates to an optoacoustic on-state; the change upon switching translates to a change of only a few percent of the original signal (Figure 3g and h). This suggests that for optoacoustic applications, photochromic rsFPs are generally much more favorable.

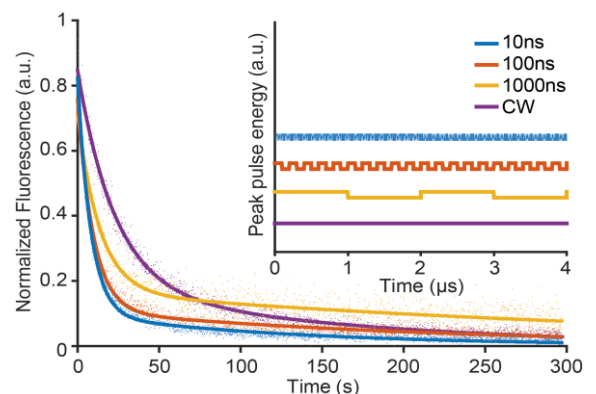


Figure 5. Dependence of the photo-fatigue of sfGFP, as an exemplary FP, on the illumination type (continuous or different types of pulsed). Used illumination patterns are depicted in the inset.

Implications for optoacoustic imaging applications employing rsFPs. In this work we comprehensively explore the characteristics of rsFPs in the context of optoacoustics. In general, photochromes are better suited for optoacoustic applications than QY-changers. Since the latter already exhibit a low QY corresponding to a high optoacoustic signal in the fluorescence ON state, the small change to an even lower QY in switched OFF state translates to a poor dynamic range for the optoacoustic signal. The dynamic range of negative-switching photochromes is directly governed by the change in absorption spectra which is often near to 100%. Due to the natural relaxation of rsFPs, the dark times of pulsed illumination effectively results in slowed switching kinetics. Thus, high-repetition laser systems are beneficial because they accelerate switching. They also reduce the number of pulses necessary for switching, decreasing overall exposure and hence photo-fatigue. rsFPs always show a faster and a slower switching kinetics, with the fast kinetics being in most cases in the direction of the equilibrium state. Ideally optoacoustic readout and switching is achieved with this wavelength using pulsed illumination and the reverse process is achieved using a second continuous illumination. This is especially true since, as demonstrated in this article, the photo-fatigue is dependent on pulse length and repetition rate. On the other hand, both on- and off-switching, kinetics for photochromic rsFPs can be used for optoacoustic readouts to gain additional CNR.

This distinct switching kinetics of rsFPs can be exploited in various optoacoustic imaging modalities, which can be classified by their penetration depth and resolution. This optoacoustic specific scalability can be approximated by the rule of thumb: penetration depth/resolution ~ 200 ⁵³. Main optoacoustic imaging modalities include high resolution optical-resolution photoacoustic microscopy (OR-PAM), acoustic-resolution photoacoustic imaging (AR-PAM), and deep penetration photoacoustic computed tomography (PACT)¹¹. The beneficial use of rsFPs for optoacoustic imaging based on the gain in CNR has already been demonstrated for OR-PAM²⁰ and PACT²⁰⁻²³. The different size of optical excited regions (focused/ full field-of-view (FOV)) influence the suitability of different rsFPs, light modulation schemes and temporal unmixing concepts.

For OR-PAM approaches the pixel dwell time is essentially governed by the switching necessary to achieve the required CNR. Scanning systems that operate with high laser repetition rates could benefit from fast transient modulation of the signal achievable by several of the fluorescence imaging optimized photochromic rsFPs. In acoustic-resolution mesoscopy systems like RSOM a broad FOV is illuminated while only single positions are read out at the acoustic focus. The approach of recording the full switching at each position results in continuous full exposure of the sample and considerable photo-fatigue. An alternative could be that the sample is continuously scanned at the acoustic focus while modulating the whole illuminated area differently by each FOV passage. Thus, sparsely capturing different points of the switching curve of each pixel reducing the total exposure and hence the photo-fatigue. The switching kinetics for each position can be delineated using locked-in detection and separating the modulated protein in the frequency domain. In this context the use of fast switching rsFPs in optoacoustic approaches operating with laser diodes³⁹ with very high repetition rates (>500 kHz) can be advantageous. For optoacoustic systems with a large FOV and an acoustic-resolution tomography approach (PACT) like MSOT⁵⁴ that operate with high laser powers and low repetition rates, full switching and temporal unmixing by difference images is a viable method. For such systems other modes of signal modulation are also conceivable, e.g. a change of the optoacoustics signal through reversible micellization leading to quenching of the signal⁵⁵.

Overall, to date switchable Bacteriophytochromes are likely the best proteins for most optoacoustic applications, due to their good dynamic range and resistance to photo-fatigue; and, foremost due to their wavelengths in the NIR, which is essential for tomography experiments with deep penetration and *in vivo* work in mammals due to the prevalence of hemoglobin as strong absorber below 700 nm. However, also very fast switching green photochromic rsFPs like Dronpa-M159T or rsEGFP2 can be beneficial for various optoacoustic imaging application. Due to the facility of boosting the CNR by temporal unmixing and the equivalent absorption spectrum to GFP, Dronpa-M159T and rsEGFP2 can directly be used as transgene labels in model organisms like *Drosophila melanogaster* pupae and adult zebrafish and thus further improve the optoacoustic imaging capabilities for morphological and functional studies in developmental biology⁵⁶.

The four rsFPs used to date for optoacoustic imaging are either designed for fluorescence or are wildtype proteins. Dedicated protein engineering of reversible switchable proteins for optoacoustic (rsOAPs) will most likely originate from Bacteriophytochromes due to their natural low QY, high absorbance and resistance to photo-fatigue and focus on accelerating their switching kinetics. Moreover, maintaining a high metastability is especially relevant for the use in low repetition rate systems. The photostability of classical green rsFPs must be improved if these proteins are to be useful. Despite the clear advantage in dynamic range of negative-switching photochromes, the surprisingly high PGE of positive-switchers remains an interesting factor. Fully photochrome positive-switching proteins could be a useful development in this direction.

CONCLUSION

To summarize, in this work we investigated the characteristics and performance of a broad range of rsFPs in optoacoustics. We provide full optoacoustic spectroscopy and switching kinetic data for all investigated proteins allowing conclusions on the influence of different switching approaches and protein characteristics on their performance as an optoacoustic label. To the best of our knowledge, this article shows the first hybrid absorption and optoacoustic spectra on optoacoustic labels. Our study provides a framework for the use of rsFP in optoacoustic imaging, which can increase the detectability and imaging contrast of transgene labels in the sample towards high penetration depth and high resolution *in vivo* optoacoustic imaging.

SUPPORTING INFORMATION

The Supporting Information is available free of charge on the ACS Publications website at DOI: XX.XXXX/acs.analchem.XXXXXXX. Supporting Information contains Supplementary Figures as indicated in the manuscript.

“VETSCHERA_Suppl_Info.pdf” contains: Multimodal Optoacoustic and Absorbance spectrometer, energy spectrum, linearity and stability of optoacoustic compounds, exemplary waveforms and frequency response, temperature in sample chamber, improvement of Optoacoustic spectra quality, optoacoustic and absorbance spectra of rsFPs in both switched states recorded concomitantly, PGE of selected proteins as a function of wavelength, OA and fluorescence signal trace of rsEGFP2 switched with 20 MHz repetition rate, exemplary optoacoustic waveforms of the reference and samples, energy spectrum for the OPO laser source used throughout the experiments, linearity and Stability of reference compounds in optoacoustic, monitoring temperature change of sample during measurement

AUTHOR INFORMATION

Corresponding Author

*E-mail: andre.stiel@helmholtz-muenchen.de.

AUTHOR CONTRIBUTIONS

PV, KM performed the experiments, analyzed the data and contributed to the manuscript. AC performed bleaching and high-repetition rate OA experiments. PV designed the OA-spectrometer setup; KM, JPFW and ACS contributed. JPFW and VN contributed to the manuscript. ACS conceived and designed the experiments and wrote the manuscript.

Notes The authors declare no competing financial interest

ACKNOWLEDGMENTS

The authors wish to thank R. Hillermann for technical assistance, L. Prade and M. Steffner for discussions and help with the bleaching experiments, as well as A.C. Rodríguez for discussions on the manuscript. The authors thank Prof. Stefan Jakobs (Max Planck Institute for Biophysical Chemistry and University of Göttingen Medical Faculty) for kindly providing several of the tested rsFPs. The authors wish to thank Vipul Gujrati for help with the thermo-camera. This work was supported by the Federal Ministry of Education and Research, Photonic Science Germany, Tech2See-13N12624, 13N12623. The work of K.M. and A.C.S. was supported by the Deutsche Forschungsgemeinschaft (STI 656/1-1).

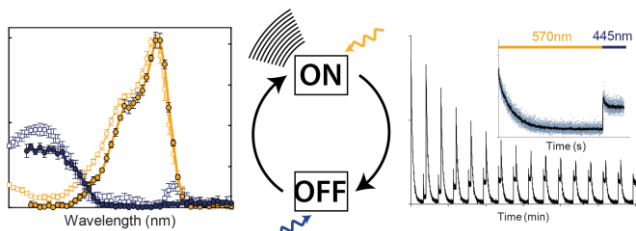
REFERENCES

- (1) Shcherbakova, D. M.; Verkhusha, V. V. Chromophore Chemistry of Fluorescent Proteins Controlled by Light. *Curr. Opin. Chem. Biol.* **2014**, *20*, 60–68.
- (2) Betzig, E. Single Molecules, Cells, and Super-Resolution Optics (Nobel Lecture). *Angew. Chem. Int. Ed. Engl.* **2015**, *54* (28), 8034–8053.
- (3) Sahl, S. J.; Hell, S. W.; Jakobs, S. Fluorescence Nanoscopy in Cell Biology. *Nat. Rev. Mol. Cell Biol.* **2017**, *18* (11), 685–701.
- (4) Zhou, X. X.; Lin, M. Z. Photoswitchable Fluorescent Proteins: Ten Years of Colorful Chemistry and Exciting Applications. *Curr. Opin. Chem. Biol.* **2013**, *17* (4), 682–690.
- (5) Nienhaus, K.; Nienhaus, G. U. Fluorescent Proteins for Live-Cell Imaging with Super-Resolution. *Chem. Soc. Rev.* **2014**, *43* (4), 1088–1106.
- (6) Duan, C.; Adam, V.; Byrdin, M.; Bourgeois, D. Structural Basis of Photoswitching in Fluorescent Proteins. *Methods Mol. Biol.* **2014**, *1148*, 177–202.
- (7) Oraevsky, A. A.; Jacques, S. L.; Tittel, F. K. Measurement of Tissue Optical Properties by Time-Resolved Detection of Laser-Induced Transient Stress. *Appl. Opt.* **1997**, *36* (1), 402–415.
- (8) Wang, L. V; Hu, S. Photoacoustic Tomography: In Vivo Imaging from Organelles to Organs. *Science* (80-.). **2012**, *335* (6075), 1458–1462.
- (9) Taruttis, A.; Ntziachristos, V. Advances in Real-Time Multispectral Photoacoustic Imaging and Its Applications. *Nat. Phot.* **2015**, *9* (4), 219–227.
- (10) Tzoumas, S.; Deliolaris, N.; Morscher, S.; Ntziachristos, V. Un-Mixing Molecular Agents from Absorbing Tissue in Multispectral Photoacoustic Tomography. *IEEE Trans. Med. Imaging* **2013**, *33* (1), 48–60.
- (11) Wang, L. V; Yao, J. A Practical Guide to Photoacoustic Tomography in the Life Sciences. *Nat. Methods* **2016**, *13* (8), 627–638.

- (12) Ntziachristos, V. Going Deeper than Microscopy: The Optical Imaging Frontier in Biology. *Nat. Methods* **2010**, *7* (8), 603–614.
- (13) Yao, J.; Wang, L.; Yang, J.-M.; Maslov, K. I.; Wong, T. T. W.; Li, L.; Huang, C.-H.; Zou, J.; Wang, L. V. High-Speed Label-Free Functional Photoacoustic Microscopy of Mouse Brain in Action. *Nat. Methods* **2015**, *12* (5), 407–410.
- (14) Wang, D.; Wu, Y.; Xia, J. Review on Photoacoustic Imaging of the Brain Using Nanoprobes. *Neurophotonics* **2016**, *3* (1), 010901.
- (15) Jokerst, J. V.; Cole, A. J.; Van de Sompel, D.; Gambhir, S. S. Gold Nanorods for Ovarian Cancer Detection with Photoacoustic Imaging and Resection Guidance via Raman Imaging in Living Mice. *ACS Nano* **2012**, *6* (11), 10366–10377.
- (16) Beziere, N.; Lozano, N.; Nunes, A.; Salichs, J.; Queiros, D.; Kostarelos, K.; Ntziachristos, V. Dynamic Imaging of PEGylated Indocyanine Green (ICG) Liposomes within the Tumor Microenvironment Using Multi-Spectral Optoacoustic Tomography (MSOT). *Biomaterials* **2015**, *37*, 415–424.
- (17) Qin, H.; Zhou, T.; Yang, S.; Chen, Q.; Xing, D. Gadolinium(III)-Gold Nanorods for MRI and Photoacoustic Imaging Dual-Modality Detection of Macrophages in Atherosclerotic Inflammation. *Nanomedicine (Lond)*. **2013**, *8* (10), 1611–1624.
- (18) Jokerst, J. V.; Thangaraj, M.; Kempen, P. J.; Sinclair, R.; Gambhir, S. S. Photoacoustic Imaging of Mesenchymal Stem Cells in Living Mice via Silica-Coated Gold Nanorods. *ACS Nano* **2012**, *6* (7), 5920–5930.
- (19) Brunker, J.; Yao, J.; Laufer, J.; Bohndiek, S. E. Photoacoustic Imaging Using Genetically Encoded Reporters: A Review. *J. Biomed. Opt.* **2017**, *22* (7), 070901.
- (20) Yao, J.; Kaberniuk, A. A.; Li, L.; Shcherbakova, D. M.; Zhang, R.; Wang, L. L. V.; Li, G.; Verkhusha, V. V.; Wang, L. L. V. Multiscale Photoacoustic Tomography Using Reversibly Switchable Bacterial Phytochrome as a Near-Infrared Photochromic Probe. *Nat. Methods* **2015**, *13* (November), 1–9.
- (21) Stiel, A. C.; Deán-Ben, X. L.; Jiang, Y.; Ntziachristos, V.; Razansky, D.; Westmeyer, G. G. High-Contrast Imaging of Reversibly Switchable Fluorescent Proteins via Temporally Unmixed Multispectral Optoacoustic Tomography. *Opt. Lett.* **2015**, *40* (3), 367–370.
- (22) Märk, J.; Dortay, H.; Wagener, A.; Zhang, E.; Buchmann, J.; Grötzinger, C.; Friedrich, T.; Laufer, J. Dual-Wavelength 3D Photoacoustic Imaging of Mammalian Cells Using a Photoswitchable Phytochrome Reporter Protein. *Commun. Phys.* **2018**, *1* (1), 3.
- (23) Deán-Ben, X. L.; Stiel, A. C.; Jiang, Y.; Ntziachristos, V.; Westmeyer, G. G.; Razansky, D. Light Fluence Normalization in Turbid Tissues via Temporally Unmixed Multispectral Optoacoustic Tomography. *Opt. Lett.* **2015**, *40* (20), 4691–4694.
- (24) Galanzha, E. E. I.; Nedosekin, D. a; Sarimollaoglu, M.; Orza, A. I.; Biris, A. S.; Verkhusha, V. V.; Zharov, V. P. Photoacoustic and Photothermal Cytometry Using Photoswitchable Proteins and Nanoparticles with Ultrasharp Resonances. *J. Biophotonics* **2013**, *13*, 1–13.
- (25) Andresen, M.; Stiel, A. C.; Trowitzsch, S.; Weber, G.; Eggeling, C.; Wahl, M. C.; Hell, S. W.; Jakobs, S. Structural Basis for Reversible Photoswitching in Dronpa. *Proc. Natl. Acad. Sci. U. S. A.* **2007**, *104* (32), 13005–13009.
- (26) Habuchi, S.; Dedecker, P.; Hotta, J.; Flors, C.; Ando, R.; Mizuno, H.; Miyawaki, A.; Hofkens, J. Photo-Induced Protonation/Deprotonation in the GFP-like Fluorescent Protein Dronpa: Mechanism Responsible for the Reversible Photoswitching. *Photochem. Photobiol. Sci.* **2006**, *5* (6), 567–576.
- (27) Shcherbakova, D. M.; Baloban, M.; Verkhusha, V. V. Near-Infrared Fluorescent Proteins Engineered from Bacterial Phytochromes. *Curr. Opin. Chem. Biol.* **2015**, *27*,

- 52–63.
- (28) Faro, A. R.; Adam, V.; Carpentier, P.; Darnault, C.; Bourgeois, D.; De Rosny, E. Low-Temperature Switching by Photoinduced Protonation in Photochromic Fluorescent Proteins. *Photochem. Photobiol. Sci.* **2010**, *9* (2), 254–262.
 - (29) Habuchi, S.; Ando, R.; Dedecker, P.; Verheijen, W.; Mizuno, H.; Miyawaki, A.; Hofkens, J. Reversible Single-Molecule Photoswitching in the GFP-like Fluorescent Protein Dronpa. **2005**, *102* (27).
 - (30) Jiménez-Banzo, A.; Nonell, S.; Hofkens, J.; Flors, C. Singlet Oxygen Photosensitization by EGFP and Its Chromophore HBDI. *Biophys. J.* **2008**, *94* (1), 168–172.
 - (31) Byrdin, M.; Duan, C.; Bourgeois, D.; Brettel, K. A Long-Lived Triplet State Is the Entrance Gateway to Oxidative Photochemistry in Green Fluorescent Proteins. *J. Am. Chem. Soc.* **2018**, *140* (8), 2897–2905.
 - (32) Kurian, E.; Prendergast, F.; Small, J. Photoacoustic Analysis of Proteins: Volumetric Signals and Fluorescence Quantum Yields. *Biophys. J.* **1997**, *73* (July), 466–476.
 - (33) Abbruzzetti, S.; Viappiani, C.; Murgida, D. H.; Erra-Balsells, R.; Bilmes, G. M. Non-Toxic, Water-Soluble Photocalorimetric Reference Compounds for UV and Visible Excitation. *Chem. Phys. Lett.* **1999**, *304* (3–4), 167–172.
 - (34) Brown, J. E.; Diaz, L.; Christoff-Tempesta, T.; Nesbitt, K. M.; Reed-Betts, J.; Sanchez, J.; Davies, K. W. Characterization of Nitrazine Yellow as a Photoacoustically Active PH Reporter Molecule. *Anal. Chem.* **2015**, *87* (7), 3623–3630.
 - (35) Peters, K. S.; Snyder, G. J. Time-Resolved Photoacoustic Calorimetry: Probing the Energetics and Dynamics of Fast Chemical and Biochemical Reactions. *Science* **1988**, *241* (4869), 1053–1057.
 - (36) Braslavsky, S. E.; Ellul, R. M.; Weiss, R. G.; Al-Ekabi, H.; Schaffner, K. Photoprocesses in Biliverdin Dimethyl Ester in Ethanol Studied by Laser-Induced Optoacoustic Spectroscopy (Lioas). *Tetrahedron* **1983**, *39* (11), 1909–1913.
 - (37) Sulfates as Chromophores for Multiwavelength Photoacoustic Imaging Phantoms. *J. Biomed. Opt.* **2017**, *22* (12), 1.
 - (38) Laufer, J.; Zhang, E.; Beard, P. Evaluation of Absorbing Chromophores Used in Tissue Phantoms for Quantitative Photoacoustic Spectroscopy and Imaging. *IEEE J. Sel. Top. Quantum Electron.* **2010**, *16* (3), 600–607.
 - (39) Stylogiannis, A.; Prade, L.; Buehler, A.; Aguirre, J.; Sergiadis, G.; Ntziachristos, V. Continuous Wave Laser Diodes Enable Fast Optoacoustic Imaging. *Photoacoustics* **2018**, *9*, 31–38.
 - (40) Ando, R.; Mizuno, H.; Miyawaki, A. Regulated Fast Nucleocytoplasmic Shuttling Observed by Reversible Protein Highlighting. *Science (80-.)*. **2004**, *1370* (2004), 1–7.
 - (41) Ando, R.; Flors, C.; Mizuno, H.; Hofkens, J.; Miyawaki, A. Highlighted Generation of Fluorescence Signals Using Simultaneous Two-Color Irradiation on Dronpa Mutants. *Biophys. J.* **2007**, *92* (12), L97-9.
 - (42) Andresen, M.; Stiel, A. C.; Fölling, J.; Wenzel, D.; Schönle, A.; Egner, A.; Eggeling, C.; Hell, S. W.; Jakobs, S. Photoswitchable Fluorescent Proteins Enable Monochromatic Multilabel Imaging and Dual Color Fluorescence Nanoscopy. *Nat. Biotechnol.* **2008**, *26* (9), 1035–1040.
 - (43) Grotjohann, T.; Testa, I.; Reuss, M.; Brakemann, T.; Eggeling, C.; Hell, S. W.; Jakobs, S. RsEGFP2 Enables Fast RESOLFT Nanoscopy of Living Cells. *Elife* **2012**, *2012* (1), 1–14.
 - (44) Stiel, A. C.; Andresen, M.; Bock, H.; Hilbert, M.; Schilde, J.; Schönle, A.; Eggeling, C.; Egner, A.; Hell, S. W.; Jakobs, S. Generation of Monomeric Reversibly Switchable Red Fluorescent Proteins for Far-Field Fluorescence Nanoscopy. *Biophys. J.* **2008**, *95* (6),

- 2989–2997.
- (45) Lavoie-Cardinal, F.; Jensen, N. a; Westphal, V.; Stiel, A. C.; Chmyrov, A.; Bierwagen, J.; Testa, I.; Jakobs, S.; Hell, S. W. Two-Color RESOLFT Nanoscopy with Green and Red Fluorescent Photochromic Proteins. *Chemphyschem* **2014**, *15* (4), 655–663.
 - (46) Subach, F. F. V; Zhang, L.; Gadella, T. T. W. J.; Gurskaya, N. G.; Lukyanov, K. a; Verkhusha, V. V; Lukyanov, A. Red Fluorescent Protein with Reversibly Photoswitchable Absorbance for Photochromic FRET. *Chem. Biol.* **2010**, *17* (7), 745–755.
 - (47) Shcherbakova, D. M.; Shemetov, A. a.; Kaberniuk, A. a.; Verkhusha, V. V. *Natural Photoreceptors as a Source of Fluorescent Proteins, Biosensors, and Optogenetic Tools*; 2014; Vol. 84.
 - (48) Ando, R.; Mizuno, H.; Miyawaki, A. Regulated Fast Nucleocytoplasmic Shuttling Observed by Reversible Protein Highlighting. *Science* **2004**, *306* (5700), 1370–1373.
 - (49) Laufer, J.; Jathoul, A.; Pule, M.; Beard, P. In Vitro Characterization of Genetically Expressed Absorbing Proteins Using Photoacoustic Spectroscopy. *Biomed. Opt. Express* **2013**, *4* (11), 2477.
 - (50) Andresen, M.; Wahl, M. C.; Stiel, A. C.; Gräter, F.; Schäfer, L. V; Trowitzsch, S.; Weber, G.; Eggeling, C.; Grubmüller, H.; Hell, S. W. Structure and Mechanism of the Reversible Photoswitch of a Fluorescent Protein. *Proc. Natl. Acad. Sci. U. S. A.* **2005**, *102* (37), 13070–13074.
 - (51) Pédelacq, J.-D.; Cabantous, S.; Tran, T.; Terwilliger, T. C.; Waldo, G. S. Engineering and Characterization of a Superfolder Green Fluorescent Protein. *Nat. Biotechnol.* **2006**, *24* (1), 79–88.
 - (52) Eggeling, C.; Volkmer, A.; Seidel, C. A. M. Molecular Photobleaching Kinetics of Rhodamine 6G by One- and Two-Photon Induced Confocal Fluorescence Microscopy. *ChemPhysChem* **2005**, *6* (5), 791–804.
 - (53) Yao, J.; Wang, L. V. Sensitivity of Photoacoustic Microscopy. *Photoacoustics* **2014**, *2* (2), 87–101.
 - (54) Ntziachristos, V.; Razansky, D. Molecular Imaging by Means of Multispectral Optoacoustic Tomography (MSOT). *Chem. Rev.* **2010**, *110* (5), 2783–2794.
 - (55) Wang, J.; Lin, C.-Y.; Moore, C.; Jhunjhunwala, A.; Jokerst, J. V. Switchable Photoacoustic Intensity of Methylene Blue via Sodium Dodecyl Sulfate Micellization. *Langmuir* **2018**, *34* (1), 359–365.
 - (56) Razansky, D.; Distel, M.; Vinegoni, C.; Ma, R.; Perrimon, N.; Köster, R. W.; Ntziachristos, V. Multispectral Opto-Acoustic Tomography of Deep-Seated Fluorescent Proteins in Vivo. *Nat. Photonics* **2009**, *3* (7), 412–417.



For TOC only